Title
Mitochondrial Stress Induces Chromatin Reorganization to Promote Longevity and UPRmt

Journal
Cell, 165(5)

ISSN
0092-8674

Authors
Tian, Ye
Garcia, Gilberto
Bian, Qian
et al.

Publication Date
2016-05-01

DOI
10.1016/j.cell.2016.04.011

Peer reviewed

HHS Public Access

Author manuscript

Cell. Author manuscript; available in PMC 2017 May 19.

Published in final edited form as:

Cell. 2016 May 19; 165(5): 1197–1208. doi:10.1016/j.cell.2016.04.011.

Mitochondrial stress induces chromatin reorganization to promote longevity and UPR^{mt}

Ye Tian[1,2], **Gilberto Garcia**[1,2], **Qian Bian**[1], **Kristan K. Steffen**[1,2], **Larry Joe**[1,2], **Suzanne Wolff**[1,2], **Barbara J. Meyer**[1], and **Andrew Dillin**[1,2,*]

[1]Howard Hughes Medical Institute and Department of Molecular and Cell Biology, University of California, Berkeley, Berkeley, CA 94720, USA

[2]The Glenn Center for Aging Research, University of California, Berkeley, Berkeley, CA 94720, USA

Summary

Organisms respond to mitochondrial stress through the upregulation of an array of protective genes, often perpetuating an early response to metabolic dysfunction across a lifetime. We find that mitochondrial stress causes widespread changes in chromatin structure through histone H3K9 di-methylation marks traditionally associated with gene silencing. Mitochondrial stress response activation requires the di-methylation of histone H3K9 through the activity of the histone methyltransferase *met-2* and the nuclear co-factor *lin-65*. While globally the chromatin becomes silenced by these marks, remaining portions of the chromatin open up, at which point the binding of canonical stress responsive factors such as DVE-1 occurs. Thus, a metabolic stress response is established and propagated into adulthood of animals through specific epigenetic modifications that allow for selective gene expression and lifespan extension.

Introduction

The fitness of an organism depends upon its capacity to adapt its metabolism in accordance with anticipated energetic demands and nutrient availability. In support of this requirement are observations that acute metabolic stresses during early development can cause persistent, widespread changes in epigenetic patterning and gene expression late in life, potentially increasing the preparedness of the organism for additional metabolic stressors. Changes in methylation patterns of chromatin caused by metabolic perturbations are often expansive and enduring, affecting long-term organismal function and occasionally permeating into

*Correspondence: ; Email: dillin@berkeley.edu

Author Contributions: Y.T. and A.D. conceived the study. Y.T. designed and performed the experiments. Y.T., G.G. and Q.B. performed immunohistochemistry experiments and data analyses on chromatin samples. Y.T., K.K.S., L.J. prepared the samples for RNA-seq and K.K.S. performed data analyses. B.M. provided expertise and ideas on chromatin analysis. Y.T., S.W. and A.D. wrote the manuscript with contributions from other authors. A.D. supervised the research.

Accession Numbers: The RNA-Seq data described in this publication have been deposited in NCBI's Gene Expression Omnibus (Edgar et al., 2002) and are accessible through GEO series accession number **GSE78252**.

subsequent generations (Jiménez-Chillarón et al., 2012). In humans, for example, *in utero* deficiency of a single nutrient, such as folate or choline, results in a massive restructuring of chromatin methylation patterns that remain visible throughout childhood (Choi and Friso, 2010). Susceptibility to obesity and diabetes in adults can be linked to dietary intake during early development and is associated with prominent modifications in chromatin (Vrachnis et al., 2012). Evidence in invertebrates further suggests that dietary-driven epigenetic modifications may permeate for generations (Rechavi et al., 2014). In each of these instances, the forced persistence of metabolic restructuring and gene expression must have a hidden adaptive value that offsets a potential loss in metabolic elasticity.

A logical regulatory center for these epigenetic phenomena lies in the mitochondria, the metabolic centers of the cell. Mitochondria are responsible for both coordinating the synthesis of NADH-donating substrates through the TCA cycle and for the production of the energy that is derived from oxidative phosphorylation. Several pieces of evidence suggest that effects of early mitochondrial dysfunction persist throughout the lifespan of the organism. For example, researchers have reported a beneficial effect of mild mitochondrial dysfunction during specific developmental stages on the lifespan of multiple organisms including the nematode *C. elegans* (Copeland et al., 2009; Dillin et al., 2002; Feng et al., 2001; Lee et al., 2003).

An important biomarker of the cellular sensing and response to this stress is a massive and persistent restructuring in gene expression patterns, as evidenced in analyses of long-lived mitochondrial mutant animals (Cristina et al., 2009; Yee et al., 2014). The upregulation of a significant portion of mitochondrial stress-responsive transcripts in *C. elegans* depends upon the activity of the transcription factor *atfs*-1, which appears to be required for the regulation of approximately half of these genes (Nargund et al., 2012). Genes regulated by *atfs*-1 are classified as part of the mitochondrial unfolded protein response, or UPR^{mt}, which includes the upregulation of mitochondrial chaperones, quality control proteases, and xenobiotic response pathway components (Nargund et al., 2012). UPR^{mt} activation also causes substantial metabolic restructuring, activating genes associated with glycolysis and repressing those associated with oxidative phosphorylation (Nargund et al., 2015). Additionally, full induction of the UPR^{mt} also requires the nuclear localization of the transcription factor *dve-1* and co-factor *ubl-5*, as well as the activity of the quality control protease *clpp-1* (Benedetti et al., 2006; Haynes et al., 2007). While the role for each of these genes in UPR^{mt} activation is well-described, the interactions among these various components at a molecular level remains ambiguous.

Histone H3K9 methylation plays a prominent role in regulating gene expression across a wide range of species (Nakayama et al., 2001; Jaenisch and Bird, 2003; González-Aguilera et al., 2014). In *C. elegans*, histone H3K9 is methylated sequentially by the methyltransferases MET-2/SETDB1 and SET-25 (Bessler et al., 2010; Towbin et al., 2012). MET-2 mono- and di-methylates H3K9 while it is still in the cytoplasm, prior to its incorporation into nucleosomes (Towbin et al., 2012). In contrast, SET-25, which is localized in the nucleus, acts as a trimethylation methyltransferase to H3K9 (Towbin et al., 2012). Collectively, these marks initiate chromatin anchoring and silencing, and are strongly associated with gene repression. H3K9me1/2 has previously been found to be critical in the

appropriate regulation of energy expenditure and fat storage (Meister et al., 2011). Additionally, subtelomeric gene silencing, mediated by the H3K36 demethylase Rph1p, is induced by mitochondrial ROS and is implicated in yeast chronological lifespan (Schroeder et al., 2013).

We find that mitochondrial stress in *C. elegans* causes widespread changes in chromatin structure, dependent on marks traditionally associated with heterochromatin. The remodeling of chromatin during stress is required for the full activation of UPR^{mt}. Chromatin reorganization requires activity of the histone methyltransferase *met-2* and a nuclear co-factor *lin-65*. While globally the chromatin becomes silenced by these marks, remaining portions of the chromatin open up, at which point binding of canonical stress responsive factors such as DVE-1 occurs. Furthermore, we find that chromatin modifications work synergistically with *atfs-1*. Collectively, our results point towards a mechanism by which early metabolic stress remodels chromatin and establishes persistent gene expression patterns.

Results

Identification of *lin-65* as a requirement for the appropriate activation of mitochondrial stress responses

We have observed that the expression of a Q40 polyglutamine tract in the neurons of *C. elegans* (*rgef-1p: :Q40: :yfp*) (Brignull et al., 2006) activates UPR^{mt} in non-neuronal tissues (Figure 1A, S1A). To identify molecular components required for this stress response, we undertook an unbiased, large-scale screen to identify genes that are required for the PolyQ-dependent activation of the UPR^{mt}. To this end, we subjected *rgef-1p: :Q40: :yfp; hsp-6p: :gfp* animals to EMS mutagenesis and analyzed 2400 mutagenized genomes for suppression of *hsp-6p: :gfp* reporter expression (an indicator of UPR^{mt} activation). We isolated 16 mutant strains that exhibited a partial or complete suppression of PolyQ dependent *hsp-6p: :gfp* expression in the F2 generation. The strong and stable suppression of the reporter GFP expression in a strain carrying the *uth2* mutation caused us to prioritize it for additional characterization (Figure S1A).

Whole genome deep sequencing (Bigelow et al., 2009; Sarin et al., 2008) identified a mutation in the *uth2* allele at amino acid 367 (GAG→AAG[Glu→Lys]) in the gene *lin-65*. Using the characterized *lin-65* mutant allele *n3441*, we confirmed that *lin-65* is required for the UPR^{mt} in response to *rgef-1p: :Q40: :yfp* expression (Figure 1A). We found that the loss in PolyQ-dependent *hsp-6p: :gfp* expression found in *lin-65* mutants was similar to that observed in *atfs-1(gk3094)* deletion strains (Figure 1A). Western blot analyses confirmed the loss of *hsp-6p: :gfp* expression in *lin-65* mutants, while PolyQ expression remained unaffected (Figure 1B). The *lin-65* mutation strongly attenuated the upregulation of the UPR^{mt} in animals fed RNAi targeting the cytochrome c oxidase-1 subunit Vb/COX4 of the electron transport chain, *cco-1*, or animals fed RNAi targeting *phb-2*, the ortholog of prohibitin PHB2 (Figure S1B). Furthermore, *lin-65* mutants exhibited a strong synthetic sterile phenotype when combined with *cco-1* RNAi (Figure 1C). The synthetic sterility was similar to that which is caused by *cco-1* RNAi in combination with loss of function of *atfs-1* (Figure 1C). Collectively, these results indicate that *lin-65* is required for UPR^{mt} activation

across a range of mitochondrial perturbations, and that *lin-65* plays an important role in the regulation of mitochondrial homeostasis.

lin-65 encodes a proline-rich protein with a low complexity domain that was originally identified as a synmuv B class gene required for vulval development in *C. elegans* (Ceol et al., 2006). LIN-65 generally lacks obvious homologous counterparts in non-nematode species, aligning most closely to a human ACRC (acidic repeat-containing) protein. To test whether *lin-65* was acting to specifically affect mitochondrial homeostasis, we examined whether *lin*-65 also played a role in the regulation of compartment-specific UPRs in either the endoplasmic reticulum (ER) or cytoplasm. We crossed the *lin-65(n3441)* mutation into animals harboring a reporter (*hsp-4p*::*gfp*) for an ER-specific stress response, the UPR^{er} (Ron and Walter, 2007). Animals were then treated with the ER-specific stressor tunicamycin, which blocks N-linked glycosylation and induces the UPR^{er} (Heifetz et al., 1979). *lin-65* did not affect the upregulation of the *hsp-4p*::*gfp* reporter by tunicamycin (Figure S1C). Similarly, we observed that *lin-65* animals were fully capable of a cytoplasmic response to a heat shock through upregulation of an *hsp-16.2p*::*gfp* reporter (Figure S1D) (Link et al., 1999). These results indicate that *lin-65* plays a specific role in the activation of mitochondrial stress responses.

Mitochondrial stress induces LIN-65 nuclear distribution

The observation that *lin*-65 is specifically required for UPR^{mt} activation suggests that the expression and/or localization of *lin-65* may be directly regulated by mitochondrial stress. To test this hypothesis, we constructed a transgenic strain expressing the 1.3kb promoter region of *lin-65* fused to the mCherry protein. We found that *lin-65* was expressed predominantly in the intestine, with weaker expression in several head neurons (Figure S2A). While *lin-65* expression was slightly upregulated in Day 1 adult animals upon *cco-1* RNAi treatment, by Day 2 this effect had dissipated, suggesting that a transcriptional upregulation of *lin-65* is not the primary mechanism by which the UPR^{mt} affects *lin-65* mediated functions (Figure S2B).

Next, to determine whether *lin-65* is post-transcriptionally regulated, we created animals in which we fused the *lin-65* cDNA between its native promoter and the mCherry fluorescent protein. *lin-65p*::*lin-65*::*mCherry* plasmid was able to rescue the suppressed UPR^{mt} induction in *lin-65(n3441)* mutants, suggesting that the fusion protein is functional (Figure S2C). Under normal conditions, intestinal *lin-65p*::*lin-65*::*mCherry* expression was diffuse in the cytosol (Figure 2A and Figure S2D). Upon *cco-1* RNAi treatment, however, *lin-65p*::*lin-65*::*mCherry* fluorescence signals strengthened and became strongly localized to the nucleus (Figure 2A). Immunoblots against transgenics in which LIN-65 was translationally fused to an HA tag further confirmed that *cco-1* RNAi was sufficient to induce LIN-65 protein expression by Day 2 of adulthood (Figure 2B) and that the signal was abolished with *lin-65* RNAi (Figure S2E). Altogether, these data suggest that the localization and protein levels of LIN-65 are regulated by mitochondrial stress.

The H3K9 methyltransferase *met-2* is required for LIN-65 nuclear accumulation induced by mitochondrial stress

Previously, *lin-65* was identified as a synmuv B class gene along with a group of chromatin modifiers (Couteau et al., 2002; Poulin et al., 2005; Ceol et al., 2006; Andersen and Horvitz, 2007). We hypothesized that one or more of these genetic interactors might influence the localization of LIN-65 in response to mitochondrial stress. Using a candidate approach against known *lin-65* genetic interactors, we examined synmuv genes for their effect on LIN-65 localization after *cco-1* RNAi treatment. We found that *met-2*, a homolog of the mammalian H3K9 methyltransferase SETDB1 (Schultz et al., 2002; Bessler et al, 2010), was required for LIN-65 nuclear accumulation during induction of the UPR^{mt}. *met-2(ok2307)* mutation strongly blocked the nuclear accumulation of *lin-65p::lin-65::mCherry* in the intestine upon *cco-1* RNAi treatment (Figure 2A). The LIN-65::HA fusion protein no longer accumulated in *met-2* mutants after treatment with *cco-1* RNAi (Figure 2C). The requirement of *met-2* for LIN-65 nuclear localization and expression suggested that epigenetic modification might also be involved in UPR^{mt} regulation. Indeed, the *met-2* mutation heavily attenuated the UPR^{mt}, in both *cco-1* and *phb-2* RNAi treated animals, as measured by *hsp-6p::gfp* induction (Figure S1B).

Global chromatin reorganization induced by mitochondrial stress is dependent on *met-2* and *lin-65*

MET-2 specifically deposits mono- and di- methyl groups on H3K9 in *C. elegans* (Towbin et al., 2012). We therefore examined whether animals with reduced ETC function exhibit changes in methylation patterns. To this end, we performed immunohistochemistry against H3K9me2 marks in germlines carrying mutations in *met-2* or *lin-65*. In agreement with previous reports, H3K9me2 level was almost undetectable in *met-2* mutants (Figure S3A). Intriguingly, however, we found that *lin-65* mutation severely reduced H3K9me2 levels as well (Figure S3A). In contrast, consistent with a role for *set-25* in H3K9me3, we observed an increase in H3K9me2 marks in *set-25* mutants (Figure S3A). *met-2* or *lin-65* mutations also abolished or severely reduced H3K9me2 methylation in intestinal cells under basal or mitochondrial stress conditions compared to wild type animals (Figure 3A and 3B). Surprisingly, we also observed striking changes in chromatin structure in intestinal nuclei upon mitochondrial stress. The intestinal nuclei appeared smaller and much more condensed in *cco-1* RNAi treated animals, while in contrast, *met-2* and *lin-65* animals had enlarged nuclei and a loose chromatin structure that remained relatively loose in structure even after mitochondrial stress was induced by *cco-1* RNAi (Figure 3A).

To directly measure nuclear size in the intestine, we used a nuclear membrane marker, *lmn-1p::emr-1::gfp*, to label intestinal nuclei (Figure 3C) (Haithcock et al., 2005). In keeping with our initial observations, we observed that the intestinal nuclear volume was significantly decreased in *cco-1* RNAi treated animals (Figure 3D) while the number and DNA content of intestinal nuclei remained unaffected (Figure S3B and S3C). Quantification of binned DAPI fractions confirmed an overall change of chromatin in *cco-1* RNAi treated animal intestinal nuclei (Figure 3E). In sum, these data suggest that mitochondrial stress induces global chromatin reorganization in addition to decreased nuclear size.

H3K9me2 is required for mitochondrial stress-induced DVE-1 nuclear puncta formation

To understand how global changes in chromatin structure may regulate UPR^{mt} induction, we next characterized the genetic interaction between the UPR^{mt} regulator DVE-1 and MET-2/LIN-65. *dve-1* encodes a homeobox domain transcription factor homologous to SATB1/SATB that translocates from the cytosol to the nucleus during mitochondrial stress (Haynes et al., 2007) (Figure 4A). To understand the interdependency of DVE-1 and LIN-65 in response to mitochondrial stress, we performed epistasis analysis in *lin-65(n3441)* animals carrying a *dve-1p*::*dve-1*::*gfp* reporter and fed *cco-1* RNAi. Strikingly, *lin-65* mutants abolished DVE-1::GFP nuclear accumulation in *cco-1* RNAi treated animals (Figure 4B). This phenotype was rescued by expression of *lin-65* with either its own promoter or an intestinal specific *gly-19* promoter (Figure S4A and S4B). These data indicate that *lin-65* is not only required but also functions cell autonomously for DVE-1 nuclear distribution under mitochondrial stress in the intestine.

During mitochondrial stress, DVE-1 not only translocates to the nucleus but also accumulates, while its mRNA level remains unaffected (Figure 4C and S4C). To further explore the role of LIN-65 in mediating the DVE-1 nuclear signal, we asked if LIN-65 also plays a role in regulating DVE-1 protein levels. Western blot analyses confirmed that DVE-1::GFP protein levels decreased in *lin-65* animals when *cco-1* RNAi was applied (Figure 4D). Similarly, *met-2* was required for DVE-1::GFP nuclear accumulation upon stress (Figure 4B and 4D). Taken together, these data indicated that LIN-65/MET-2 are specifically required for mitochondrial stress-induced DVE-1 nuclear distribution and expression.

During these experiments, we also noticed that the DVE-1::GFP fusion protein formed punctate structures in the nucleus during mitochondrial stress (Figure 4B and S4D) (Haynes et al., 2007). In comparison, the intensity of nuclear DVE-1::GFP signal decreased in both *lin-65* and *met-2* animals fed *cco-1* RNAi (Figure S4D) and fewer cells contained detectable DVE-1::GFP puncta (Figure 4E and Figure S4D). To resolve the specific areas in which DVE-1 puncta were localized in the nucleus, we performed immunohistochemistry with H3K9me2 antibody in DVE-1::GFP animals fed *cco-1* RNAi. We did not observe co-localization between DVE-1 puncta and the H3K9me2 signal (Figure S4E). Instead, however, we found that the DVE-1::GFP puncta reside in the weak DAPI staining region, surrounded by condensed chromatin that exhibit strong DAPI staining (Figure 4F, 4G). To globally quantify this phenotype, we analyzed the relative ratios of GFP and DAPI intensity in different regions of the nucleus. Consistently, DVE-1::GFP signals were significantly enriched in regions of the nucleus exhibiting low levels of DAPI signal, while depleted from regions exhibiting strong DAPI staining signals (Figure 4H). Collectively, these results indicate that DVE-1::GFP puncta are preferentially localized in nuclear compartments devoid of condensed chromatin where gene expression is predicted to be most active.

Because both H3K9me2 and H3K9me3 are important for heterochromatin formation and gene silencing, we tested whether *set-25* has a similar effect on DVE-1 localization upon mitochondrial stress. To this end, we monitored nuclear DVE-1::GFP localization in *set-25(n5021)* mutants in which H3K9me2 levels are elevated (Figure S3A). Remarkably, we observed an opposing phenotype: *set-25* mutants increased DVE-1::GFP nuclear

localization even in the absence of mitochondrial stress (Figure S5A). The DVE-1: :GFP accumulation in *set-25* mutants, however, was neither required for *cco-1* RNAi induced longevity nor sufficient for lifespan extension (Figure S5B and Table S1). These results suggest that H3K9me2 is specifically required for DVE-1 nuclear accumulation in response to mitochondrial stress.

lin-65 functions in development to establish UPR^{mt} induction

To understand whether LIN-65 is required for establishing or perpetuating UPR^{mt} into adulthood, we tested the timing requirements of *lin-65* in mediating DVE-1 puncta formation. Animals in which mitochondrial stress was induced during development (*cco-1* RNAi during development), but which had *lin-65* reduced only during adulthood retained nuclear DVE-1: :GFP puncta formation (Figure 4I). In contrast, animals with both mitochondrial stress and reduced *lin-65* activity only during development completely suppressed DVE-1: :GFP puncta formation in adulthood (Figure 4I). These data indicate that *lin-65* likely establishes an epigenetic mark on H3K9 during development, allowing for DVE-1 puncta formation in response to mitochondrial stress.

lin-65 and *met-2* are required for regulating the transcriptional response to mitochondrial stress

To understand the role of *lin-65* and *met-2* in regulating the transcriptional response to mitochondrial stress, we performed RNA-seq on wild type, *lin-65* and *met-2* animals, each in the presence or absence of *cco-1* RNAi. In wild type animals, our analysis identified 1312 genes that were differentially expressed in the *cco-1* RNAi treated condition relative to animals grown on empty vector bacteria (Benjamini adjusted p-value < 0.05) (Figure 5A, S6A, Table S2). Using qPCR, we confirmed that *hsp-6* and *timm-23* induction by *cco-1* RNAi were perpetuated throughout adulthood (Figure 5B), consistent with epigenetic modifications induced by *cco-1* being sufficient to ensure target gene expression long after establishing chromatin marks during development. In the absence of *lin-65* and *met-2*, many *cco-1* regulated genes exhibited wide variance in expression patterns and failed to become significantly changed from their expression on empty vector. In fact, a majority of the gene expression changes (884 up-regulated genes and 380 down-regulated genes) induced by *cco-1* RNAi were abrogated in *lin-65* or *met-2* mutant animals (Figure 5A, S6A, S6B and Table S2) (see Discussion). These data demonstrate that proper regulation of gene expression in response to *cco-1* RNAi is dependent upon the chromatin reorganization activities of *lin-65* and *met-2* and that the global changes in gene expression due to mitochondrial stress are dependent upon the function of LIN-65 and/or MET-2.

The nuclear localization of LIN-65 is partially dependent on CLPP-1/DVE-1 and independent of ATFS-1

We next asked whether the function of additional UPR^{mt} components were required for LIN-65's expression and/or nuclear localization. The most proximal responders to mitochondrial stress required to induce the UPR^{mt} are the mitochondrial protease, *clpp-1*, and the transcription factor *dve-1* (Haynes et al., 2007). We found that RNAi against *clpp-1* or *dve-1* strongly suppressed LIN-65 nuclear translocation as well as protein expression under both normal and mitochondrial stress conditions (Figure 6A, 6B and S7A). This

suggested that a reciprocal, interdependent relationship exists between DVE-1 and LIN-65 for their expression and localization.

Much like LIN-65, ATFS-1 exhibits dual localization in the cell, increasing its propensity toward nuclear localization under mitochondrial stress, during which it is responsible for the transcriptional upregulation of an array of genes that protect from protein unfolding, bacterial pathogenesis, and cholesterol deprivation (Nargund et al., 2012). Intriguingly, we found that loss of *atfs-1*, which is sufficient to abolish UPR^{mt}, does not affect the nuclear localization of LIN-65 or chromatin compaction induced by *cco-1* RNAi (Figure 6A and S7B). In fact, *atfs-1* RNAi actually enhanced LIN-65 protein levels under both normal and mitochondrial stress conditions (Figure 6B and S7A). These data suggest that multiple parallel pathways, regulated by both CLPP-1/LIN-65/DVE-1 and ATFS-1, are required for overall regulation of UPR^{mt}.

lin-65/met-2 and *atfs-1* are required for mitochondrial stress-induced longevity

Mitochondrial stress induced by *cco-1* RNAi during development increases lifespan and induces the UPR^{mt} (Dillin et al., 2002, Durieux et al., 2011). To test whether *lin-65* is required for lifespan extension upon mitochondrial stress, we assayed the lifespan of *lin-65* animals with or without *cco-1* RNAi. Both *lin-65* and *met*-2 animals are short lived under normal conditions. As predicted, both *lin-65(n3441)* and *met-2(ok2307)* only partially suppressed the lifespan extension of *cco-1* RNAi treated animals (Figure 6C-D and Table S1). We hypothesized that perhaps a redundancy with *atfs-1* function on lifespan was driving the incomplete suppression of lifespan in these experiments. To test this, we assayed the lifespan of *met-2* animals with or without *cco-1* RNAi in combination with *atfs-1* RNAi. Like *met-2* and *lin-65*, *atfs-1* RNAi alone was incapable of fully suppressing the extension of lifespan in *cco-1* RNAi animals (Figure 6D and Table S1). *afts-1* RNAi also did not further decrease the lifespan of wild type or *met-2* mutant animals under normal conditions (Figure 6D and Table S1). Importantly, however, *atfs-1* RNAi further decreased the lifespan extension of *met-2; cco-1* RNAi treated animals to the level of wild type animals (Figure 6E and Table S1), suggesting that *met-2* and *atfs-1* function synergistically to mediate mitochondrial stress-induced longevity.

Together, these data suggest that mitochondrial stress during development is sufficient to initiate a cascade of events, including *met-2* dependent H3K9me2 methylation, LIN-65 nuclear accumulation, chromatin reorganization and DVE-1 nuclear punctate structure formation, in addition to nuclear localization of the mitochondrial stress specific transcription factor ATFS-1 (Figure 7A-G). Collectively, this cascade of responses works to initiate beneficial changes in gene expression that are perpetuated into adulthood. Thus, chromatin reorganization and induction of the UPR^{mt} function synergistically to regulate mitochondrial stress-induced longevity.

Discussion

We have taken advantage of a cell non-autonomous mitochondrial stress model that elicits mild mitochondrial dysfunction to identify the genetic requirements of UPR^{mt} induction, identifying *lin-65/met-2* as integral parts of the UPR^{mt} signaling pathway. We believe that

the model by which this occurs will be complex: due to the fact that LIN-65 translocates from the cytosol to the nucleus upon mitochondrial stress as well as H3K9me2 being produced in the cytosol where MET-2 is present (Towbin et al., 2012) and the possibility that *lin-65* plays a pivotal role in nucleosome/histone exchange in the nucleus in order for the H3K9me2 marks to appear on the chromatin at the proper loci upon mitochondrial stress. Whether LIN-65 is able to directly bind histone H3 in the cytoplasm, and how it is involved in H3K9 di-methylation are yet to be determined.

Nuclear H3K9me2 levels do not increase in the presence of mitochondrial stress, although nuclear LIN-65 accumulation does. One possible explanation for this observance is that LIN-65's function is not limited to the potential shuttling of H3K9me2 subunits to the nucleus, but plays a more definitive role in the deposition or localization of the H3K9me2 subunit onto the chromatin under mitochondrial stress. Therefore, it is not the total accumulation of H3K9me2 in the nucleus that determines UPR^{mt} induction and longevity, but rather the appropriate localization and utilization of this subunit to form precise chromatin structures for gene regulation. Likewise, in the absence of mitochondrial stress, loss of *lin-65* results in a significant reduction of nuclear H3K9me2, although LIN-65 has not accumulated in the nucleus. If indeed LIN-65 is required to shuttle and distribute H3K9me2 subunits in the nucleus, under non-stressed conditions LIN-65 continues to shuttle to the nucleus, but is not retained and does not accumulate. The lack of LIN-65 in the nucleus during non-stressed conditions could result in release of the H3K9me2 subunits and their conversion to H3K9me1/3 or degradation. Alternatively, loss of *lin-65* may result in a subset of H3K9me2 subunits in the cytoplasm accumulating that negatively impact MET-2 activity.

DVE-1 was previously identified as an UPR^{mt} regulator found at the promoters of UPR^{mt} target genes in mitochondrial-stressed *C. elegans* (Haynes et al., 2007). In this study, we find there is interdependency between LIN-65 and DVE-1 for their nuclear localization and to maintain their protein levels during mitochondrial stress. It is possible that cells may benefit from this dependency to elicit intricate chromatin remodeling and gene regulation in response to the specific stress signals. Future studies will help determine the relative contributions of protein stability and translation on LIN-65 and DVE-1 expression patterns.

Under energy depleted conditions, silencing of gene expression by active global chromatin condensation will conserve energy required for the timely activation of mitochondrial stress related genes, thereby ensuring an adequate stress response optimal for survival. Interestingly, we noticed that DVE-1 forms puncta upon mitochondrial stress, which only reside in the loose chromatin regions where DAPI staining is weak. Similarly, a special AT-rich binding protein SATB1 (a mammalian homolog of DVE-1) also locates in regions devoid of condensed chromatin (Cai et al., 2003). SATB1 plays a key role in organization of the chromatin “loopscape” that allows for the regulation of gene expression at a distance (Galande et al., 2007, Yasui et al., 2002). It is likely that mitochondrial stress induces global changes in high order chromatin structure through H3K9me2, which passively forces DVE-1 to the more assessable regions on the chromatin open for gene expression. Alternatively, other histone modifications or chromatin modifying factors might be directly recruiting DVE-1 to the determined positions.

Studies in yeast have shown that subtelomeric silencing can mediate mitochondrial ROS-induced chronological longevity, propagating heterochromatin formation near telomere regions and regulating post-mitotic cellular health (Schroeder et al., 2013). Because the chromatin marks found in yeast undergoing ROS-induced damage are distinct from the chromatin marks found in this study using reduced ETC, we hypothesize that mitochondrial stressors may act via highly specific mechanisms to coordinate the activation of the protective pathways best suited to the mitochondrial damage at hand. In future studies, it will be interesting to compare the chromatin status across different forms of mitochondrial stress to understand the extent to which they correlate with lifespan extension.

Our RNA-Seq analysis identified a large set of genes that were differentially expressed in response to *cco-1* RNAi treatment, establishing this set of genes as being pivotal for animals to thrive in the face of mitochondrial stress. Although the overwhelming majority of *cco-1* induced gene expression changes were abrogated upon loss of *lin-65* or *met-2*, many exhibited mean expression changes that were qualitatively similar to that seen in wild type animals (Figure S6A). This is particularly true for the down-regulated genes in the *lin-65* mutant (Figure S6A). Importantly, many of the genes we analyzed exhibited increased variability within biological replicates in the *lin-65* and *met-2* mutant animals (Figure S6B, Table S2), limiting the statistical significance for many gene expression changes. In general, the variance among biological replicates was increased in the *lin-65* and *met-2* mutants relative to wild type, despite careful handling and harvesting of each of the replicate sets together. Among the possible explanations for increased variance in these mutants, we favor a model where loss of *lin-65* or *met-2* results in increased transcriptional noise, which is consistent with previous reports that the chromatin environment can epigenetically regulate transcriptional noise in diverse systems (Hansen and O'Shea, 2013, Anderson et al., 2014, Lavigne et al., 2015, Dey et al., 2015). While it will be important to formally address this hypothesis in the future, the data presented here clearly emphasize the importance of *lin-65* and *met-2* in properly orchestrating the chromatin in order to mount an appropriate response to mitochondrial stress.

The impacts of early life stress on the long-term well-being of an organism, especially in the progression of the aging process, have been long debated. The fact that the mitochondrial stress experienced early during development extends lifespan indicates that these animals might possess an epigenetic mechanism to ensure the beneficial effects from such stress are maintained throughout the lifespan. Such a mechanism seems to be carried out by both H3K9 methylation and DVE-1 mediated chromatin structure changes in peripheral tissues.

Experimental Procedures

Strains

SJ4100 (zcIs13[*hsp-6p*: :*gfp*]), CL2070 (dvIs70[*hsp-16.2p*: :*gfp*]), SJ4005 (zcIs4[*hsp-4p*: :*gfp*]), SJ4197 (zcIs39[*dve-1p*: :*dve-1*: :*gfp*]), MR142 (*cdc-25.1(rr31)*; rrIs1 [*elt-2*: :*gfp* + *unc-119*(+)]), MT13232 (*lin-65(n3441)*), RB1789 (*met-2(ok2307)*), MT17463 (*set-25(n5021)*), LW699 (jjIs699[*lmn-1p*: :*emr-1*: :*gfp*] and N2 wild type strains were obtained from the Caenorhabditis Genetics Center (Minneapolis, MN). AM101

(rmIs101[*rgef-1p*::*Q40*::*yfp*]) was a generous gift from Rick Morimoto. VC3201 (*atfs-1(gk3094)*) was obtained from the National BioResource Project (Tokyo, Japan).

AGD1491 (uthIs400 [*lin-65p*::*mCherry*::*unc-54* 3′UTR; pRF4(*rol-6*)]) (6×),

AGD1492 (uthIs401 [*lin-65p*::*lin-65cDNA*::*mCherry*::*unc-54* 3′UTR; pRF(*rol-6*)]) (6×),

AGD1540 (uthIs432 [*lin-65p*::*lin-65cDNA*::*HA*::*unc-54 3′UTR*; pRF4(*rol-6*)]) (3×),

AGD1540 (uthIs433 [*lin-65p*::*lin-65cDNA*::*HA*::*unc-54 3′UTR*; pRF4(*rol-6*)]) (3×)

For generation of *lin-65p*::*mCherry* strain, the *lin-65* 1.3kb promoter was PCR amplified from genomic DNA and cloned into pNB23(*sur-5p*::*mCherry*) using SphI and XmaI. For the *lin-65p*::*lin-65cDNA*::*mCherry* strain, the *lin-65* cDNA(2184bp) without stop codon was inserted into *lin-65p*::mCherry construct with XmaI and XbaI. *lin-65* cDNA was a gift from Robert Horvitz. For the generation of *lin-65p*::*lin-65cDNA*::*HA* transgenic worms, the *mCherry*::*unc-5*4 3′UTR was replaced by HA-tag::*unc-54* 3′UTR using XbaI and ApaI. To replace the *lin-65* promoter, the *gly-19* promoter was cloned in place of the *lin-65* promoter in the *lin-65p*::*lin-65 cDNA*::*mCherry* plasmid. Transgenic strains were generated by microinjecting target constructs (70ng/ul) mixed with a pRF4(*rol-6*) (50ng/ul) co-injection marker. Extrachromosomal arrays were integrated using irradiation and backcrossed 3-6 times.

RNAi feeding

Worms were grown from hatch on HT115 *E. coli* containing an empty vector control or expressing double-stranded RNA. RNAi strains were from the Vidal library if present, or the Ahringer library if absent from the Vidal library.

Western blot Analysis

Age synchronized worms were grown on plates containing HT115 RNAi bacteria at 20°C. For large-scale experiments, worms were washed off the plate with M9 buffer and worm pellets were frozen in liquid nitrogen for further processing. Worm extracts were generated by glass bead disruption in non-denaturing lysis buffer [150 mM NaCl, 50 mM Hepes at pH 7.4, 1mM EDTA, 1% Triton X100, protease inhibitor cocktail III (Calbiochem)]. For small-scale experiments, 120 worms were picked into 14ul M9 buffer and frozen in liquid nitrogen. 6×SDS loading buffer and 10× reducing reagent were added to each sample. Samples were boiled for 15 mins and resolved by NuPAGE Bis-Tris mini gels.

Antibodies

Antibodies used for Western blot and IF were as follows: anti-GFP antibody (Roche 11814460001), anti-Tubulin antibody (Sigma T6074); anti-HA-Tag (C29F4) Rabbit mAb #3724; anti-Histone H3 (di methyl K9) antibody (mAbcam 1220)

Lifespan analysis

Lifespan experiments were performed at 20°C as previously described (Dillin et al., 2002). Worms were synchronized by egg bleach and grown on *E. coli* HT115 for RNAi from hatch.

Worms were scored every second day. Prism5 software was used for statistical analysis. Log-rank (Mantel-Cox) method was used to determine the significance difference.

Supplementary Material

Refer to Web version on PubMed Central for supplementary material.

Acknowledgments

We thank the *Caenorhabditis* Genetic Center and Shohei Mitani of the National BioResource Project for providing strains. We also thank Dr. Robert Horvitz for providing the *lin-65* cDNA plasmid. We are grateful to Tao Cai at NIBS for the help with whole genome deep sequencing data analyses. This work used the Vincent J. Coates Genomics Sequencing Laboratory at UC Berkeley, supported by NIH S10 Instrumentation Grants S10RR029668 and S10RR027303. This work used the CRL Molecular Imaging Center, supported by Gordon and Betty Moore Foundation. Y.T. was supported by the Glenn Foundation for Medical Research Postdoctoral Fellowship. K.K.S. was supported by a grant from the Jane Coffin Childs Memorial Fund for Medical Research. S.W. received support from the Glenn Foundation for Medical Research. This work was also supported by the NIH grant (R37 AG024365) and HHMI. A.D. is a founder of Proteostasis Therapeutics and Mitobridge, inc. and declares no financial interest.

References

Andersen EC, Horvitz HR. Two C. elegans histone methyltransferases repress lin-3 EGF transcription to inhibit vulval development. Dev Camb Engl. 2007; 134:2991–2999.

Anderson MZ, Gerstein AC, Wigen L, Baller JA, Berman J. Silencing is noisy: population and cell level noise in telomere-adjacent genes is dependent on telomere position and sir2. PLoS Genet. 2014; 10:e1004436. [PubMed: 25057900]

Benedetti C, Haynes CM, Yang Y, Harding HP, Ron D. Ubiquitin-like protein 5 positively regulates chaperone gene expression in the mitochondrial unfolded protein response. Genetics. 2006; 174:229–239. [PubMed: 16816413]

Bessler JB, Andersen EC, Villeneuve AM. Differential localization and independent acquisition of the H3K9me2 and H3K9me3 chromatin modifications in the Caenorhabditis elegans adult germ line. PLoS Genet. 2010; 6:e1000830. [PubMed: 20107519]

Bigelow H, Doitsidou M, Sarin S, Hobert O. MAQGene: software to facilitate C. elegans mutant genome sequence analysis. Nat Methods. 2009; 6:549. [PubMed: 19620971]

Brignull HR, Moore FE, Tang SJ, Morimoto RI. Polyglutamine proteins at the pathogenic threshold display neuron-specific aggregation in a pan-neuronal Caenorhabditis elegans model. J Neurosci Off J Soc Neurosci. 2006; 26:7597–7606.

Cai S, Han HJ, Kohwi-Shigematsu T. Tissue-specific nuclear architecture and gene expression regulated by SATB1. Nat Genet. 2003; 34:42–51. [PubMed: 12692553]

Ceol CJ, Stegmeier F, Harrison MM, Horvitz HR. Identification and Classification of Genes That Act Antagonistically to let-60 Ras Signaling in Caenorhabditis elegans Vulval Development. Genetics. 2006; 173:709–726. [PubMed: 16624904]

Choi SW, Friso S. Epigenetics: A New Bridge between Nutrition and Health. Adv Nutr Int Rev J. 2010; 1:8–16.

Copeland JM, Cho J, Lo T Jr, Hur JH, Bahadorani S, Arabyan T, Rabie J, Soh J, Walker DW. Extension of Drosophila Life Span by RNAi of the Mitochondrial Respiratory Chain. Curr Biol. 2009; 19:1591–1598. [PubMed: 19747824]

Couteau F, Guerry F, Müller F, Palladino F. A heterochromatin protein 1 homologue in Caenorhabditis elegans acts in germline and vulval development. EMBO Rep. 2002; 3:235–241. [PubMed: 11850401]

Cristina D, Cary M, Lunceford A, Clarke C, Kenyon C. A Regulated Response to Impaired Respiration Slows Behavioral Rates and Increases Lifespan in Caenorhabditis elegans. PLoS Genet. 2009; 5:e1000450. [PubMed: 19360127]

Dey SS, Foley JE, Limsirichai P, Schaffer DV, Arkin AP. Orthogonal control of expression mean and variance by epigenetic features at different genomic loci. Mol Syst Biol. 2015; 11:806. [PubMed: 25943345]

Dillin A, Hsu AL, Arantes-Oliveira N, Lehrer-Graiwer J, Hsin H, Fraser AG, Kamath RS, Ahringer J, Kenyon C. Rates of Behavior and Aging Specified by Mitochondrial Function During Development. Science. 2002; 298:2398–2401. [PubMed: 12471266]

Durieux J, Wolff S, Dillin A. The Cell Non-Autonomous Nature of Electron Transport Chain-Mediated Longevity. Cell. 2011; 144:79–91. [PubMed: 21215371]

Edgar R, Domrachev M, Lash AE. Gene Expression Omnibus: NCBI gene expression and hybridization array data repository. Nucleic Acids Res. 2002; 30:207–210. [PubMed: 11752295]

Feng J, Bussière F, Hekimi S. Mitochondrial electron transport is a key determinant of life span in Caenorhabditis elegans. Dev Cell. 2001; 1:633–644. [PubMed: 11709184]

Galande S, Purbey PK, Notani D, Kumar PP. The third dimension of gene regulation: organization of dynamic chromatin loopscape by SATB1. Curr Opin Genet Dev. 2007; 17:408–414. [PubMed: 17913490]

González-Aguilera C, Palladino F, Askjaer P. C. elegans epigenetic regulation in development and aging. Brief Funct Genomics. 2014; 13:223–234. [PubMed: 24326118]

Haithcock E, Dayani Y, Neufeld E, Zahand AJ, Feinstein N, Mattout A, Gruenbaum Y, Liu J. Age-related changes of nuclear architecture in Caenorhabditis elegans. Proc Natl Acad Sci U S A. 2005; 102:16690–16695. [PubMed: 16269543]

Hansen AS, O'Shea EK. Promoter decoding of transcription factor dynamics involves a trade-off between noise and control of gene expression. Mol Syst Biol. 2013; 9:704. [PubMed: 24189399]

Haynes CM, Petrova K, Benedetti C, Yang Y, Ron D. ClpP mediates activation of a mitochondrial unfolded protein response in C. elegans. Dev Cell. 2007; 13:467–480. [PubMed: 17925224]

Heifetz A, Keenan RW, Elbein AD. Mechanism of action of tunicamycin on the UDP-GlcNAc:dolichyl-phosphate GlcNAc-1-phosphate transferase. Biochemistry (Mosc). 1979; 18:2186–2192.

Jaenisch R, Bird A. Epigenetic regulation of gene expression: how the genome integrates intrinsic and environmental signals. Nat Genet. 2003; 33:245–254. [PubMed: 12610534]

Jiménez-Chillarón JC, Díaz R, Martínez D, Pentinat T, Ramón-Krauel M, Ribó S, Plösch T. The role of nutrition on epigenetic modifications and their implications on health. Biochimie. 2012; 94:2242–2263. [PubMed: 22771843]

Lavigne MD, Vatsellas G, Polyzos A, Mantouvalou E, Sianidis G, Maraziotis I, Agelopoulos M, Thanos D. Composite macroH2A/NRF-1 Nucleosomes Suppress Noise and Generate Robustness in Gene Expression. Cell Rep. 2015; 11:1090–1101. [PubMed: 25959814]

Lee SS, Lee RYN, Fraser AG, Kamath RS, Ahringer J, Ruvkun G. A systematic RNAi screen identifies a critical role for mitochondria in C. elegans longevity. Nat Genet. 2003; 33:40–48. [PubMed: 12447374]

Link CD, Cypser JR, Johnson CJ, Johnson TE. Direct observation of stress response in Caenorhabditis elegans using a reporter transgene. Cell Stress Chaperones. 1999; 4:235–242. [PubMed: 10590837]

Meister P, Schott S, Bedet C, Xiao Y, Rohner S, Bodennec S, Hudry B, Molin L, Solari F, Gasser SM, et al. Caenorhabditis elegans Heterochromatin protein 1 (HPL-2) links developmental plasticity, longevity and lipid metabolism. Genome Biol. 2011; 12:R123. [PubMed: 22185090]

Nakayama J, Rice JC, Strahl BD, Allis CD, Grewal SIS. Role of Histone H3 Lysine 9 Methylation in Epigenetic Control of Heterochromatin Assembly. Science. 2001; 292:110–113. [PubMed: 11283354]

Nargund AM, Pellegrino MW, Fiorese CJ, Baker BM, Haynes CM. Mitochondrial import efficiency of ATFS-1 regulates mitochondrial UPR activation. Science. 2012; 337:587–590. [PubMed: 22700657]

Nargund AM, Fiorese CJ, Pellegrino MW, Deng P, Haynes CM. Mitochondrial and Nuclear Accumulation of the Transcription Factor ATFS-1 Promotes OXPHOS Recovery during the UPR(mt). Mol Cell. 2015; 58:123–133. [PubMed: 25773600]

Poulin G, Dong Y, Fraser AG, Hopper NA, Ahringer J. Chromatin regulation and sumoylation in the inhibition of Ras-induced vulval development in Caenorhabditis elegans. EMBO J. 2005; 24:2613–2623. [PubMed: 15990876]

Rechavi O, Houri-Ze'evi L, Anava S, Goh WSS, Kerk SY, Hannon GJ, Hobert O. Starvation-Induced Transgenerational Inheritance of Small RNAs in C. elegans. Cell. 2014; 158:277–287. [PubMed: 25018105]

Ron D, Walter P. Signal integration in the endoplasmic reticulum unfolded protein response. Nat Rev Mol Cell Biol. 2007; 8:519–529. [PubMed: 17565364]

Sarin S, Prabhu S, O'Meara MM, Pe'er I, Hobert O. Caenorhabditis elegans mutant allele identification by whole-genome sequencing. Nat Methods. 2008; 5:865–867. [PubMed: 18677319]

Schroeder EA, Raimundo N, Shadel GS. Epigenetic Silencing Mediates Mitochondria Stress-induced Longevity. Cell Metab. 2013; 17:954–964. [PubMed: 23747251]

Schultz DC, Ayyanathan K, Negorev D, Maul GG, Rauscher FJ. SETDB1: a novel KAP-1-associated histone H3, lysine 9-specific methyltransferase that contributes to HP1-mediated silencing of euchromatic genes by KRAB zinc-finger proteins. Genes Dev. 2002; 16:919–932. [PubMed: 11959841]

Towbin BD, González-Aguilera C, Sack R, Gaidatzis D, Kalck V, Meister P, Askjaer P, Gasser SM. Step-wise methylation of histone H3K9 positions heterochromatin at the nuclear periphery. Cell. 2012; 150:934–947. [PubMed: 22939621]

Vrachnis N, Antonakopoulos N, Iliodromiti Z, Dafopoulos K, Siristatidis C, Pappa KI, Deligeoroglou E, Vitoratos N. Impact of Maternal Diabetes on Epigenetic Modifications Leading to Diseases in the Offspring. J Diabetes Res. 2012; 2012:e538474.

Yasui D, Miyano M, Cai S, Varga-Weisz P, Kohwi-Shigematsu T. SATB1 targets chromatin remodelling to regulate genes over long distances. Nature. 2002; 419:641–645. [PubMed: 12374985]

Yee C, Yang W, Hekimi S. The Intrinsic Apoptosis Pathway Mediates the Pro-Longevity Response to Mitochondrial ROS in C. elegans. Cell. 2014; 157:897–909. [PubMed: 24813612]

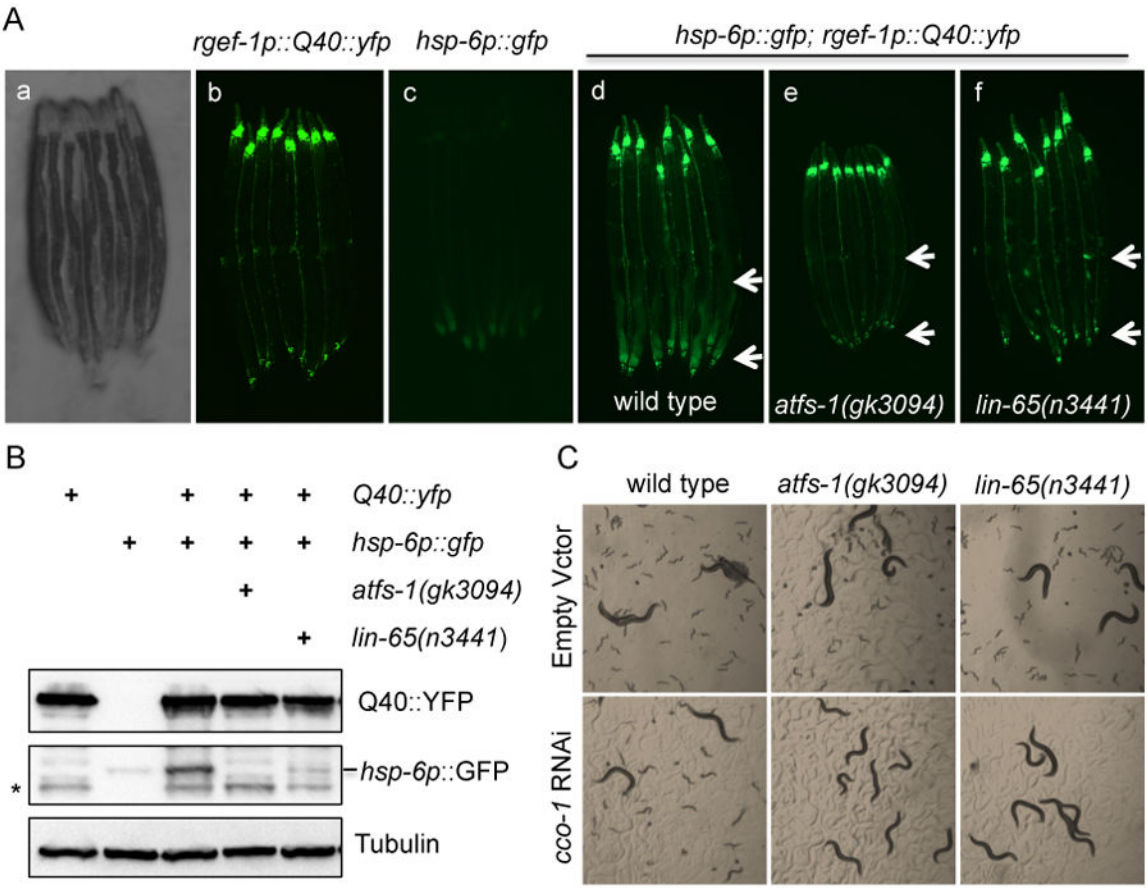

Figure 1. Neuronal polyglutamine expression induces a *lin*-65 dependent activation of the UPR^{mt}

(A) Representative photomicrographs demonstrating: a) bright field image of aligned, wild type worms; b) YFP expression in the neurons; c) *hsp-6p*: :*gfp* expression in wild type (WT) animals; d) *hsp-6p*: :*gfp* is induced in the intestine in *rgef-1p*: :*Q40*: :*yfp* animals; e) *hsp-6p*: :GFP suppression in *atfs-1* animals; f) *hsp-6p*: :GFP suppression in *lin-65* animals. Arrows indicate the posterior region of the intestine where *hsp-6p*: :*gfp* is induced or suppressed. See also Figure S1.

(B) Immunoblots of GFP expression in *hsp-6p*: :*gfp*; *rgef-1p*: :*Q40*: :*yfp* animals in the presence or absence of *atfs-1* or *lin-65* mutation. Anti-tubulin serves as a loading control. * indicates a cleaved band from Q40: :YFP that is recognized by GFP antibody.

(C) Representative photomicrographs of WT, *atfs-1* and *lin-65* animals grown on EV or *cco-1* RNAi from hatch.

Day 2 of adulthood animals were used for imaging and western blots analyses.

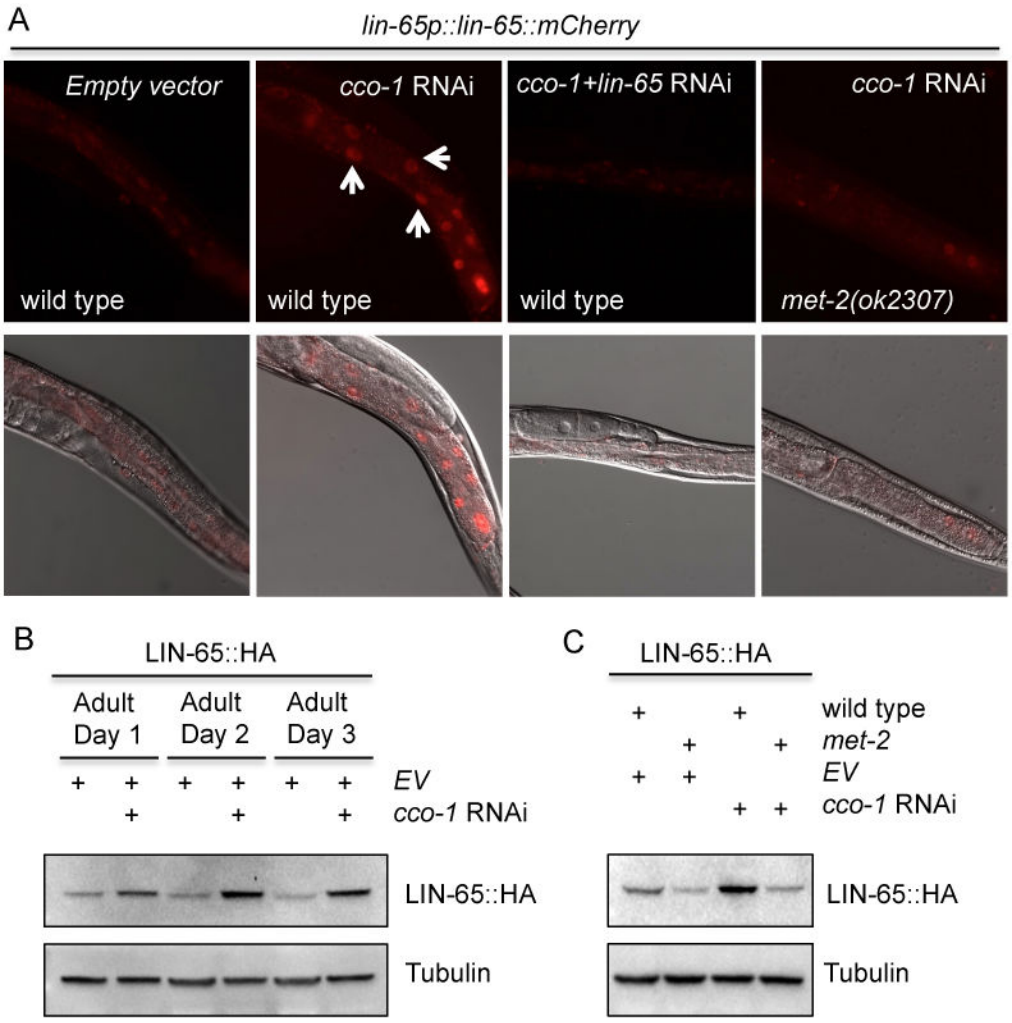

Figure 2. The *C. elegans* histone H3K9me1/2 methyltransferase *met-2* is required for LIN-65 nuclear accumulation upon *cco-1* RNAi

(A) Representative photomicrographs of *lin-65p*::*lin-65*::*mCherry* animals in a WT or *met-2* mutant background grown on EV, *cco-1* RNAi, or *cco-1+lin-65* double RNAi bacteria from hatch (as indicated). Images were taken at day 1 of adulthood. Arrows indicate intestinal nuclei.

(B) Immunoblot of LIN-65::HA expression in animals grown on EV and EV+*cco-1* RNAi from hatch as indicated. Animals were collected at Day 1, 2 and 3 of adulthood. Anti-tubulin serves as a loading control.

(C) Immunoblot of LIN-65::HA expression in WT or *met-2* mutants grown on EV or *cco-1* RNAi (as indicated) from hatch. Animals were collected at Day 2 of adulthood. Anti-tubulin serves as a loading control.

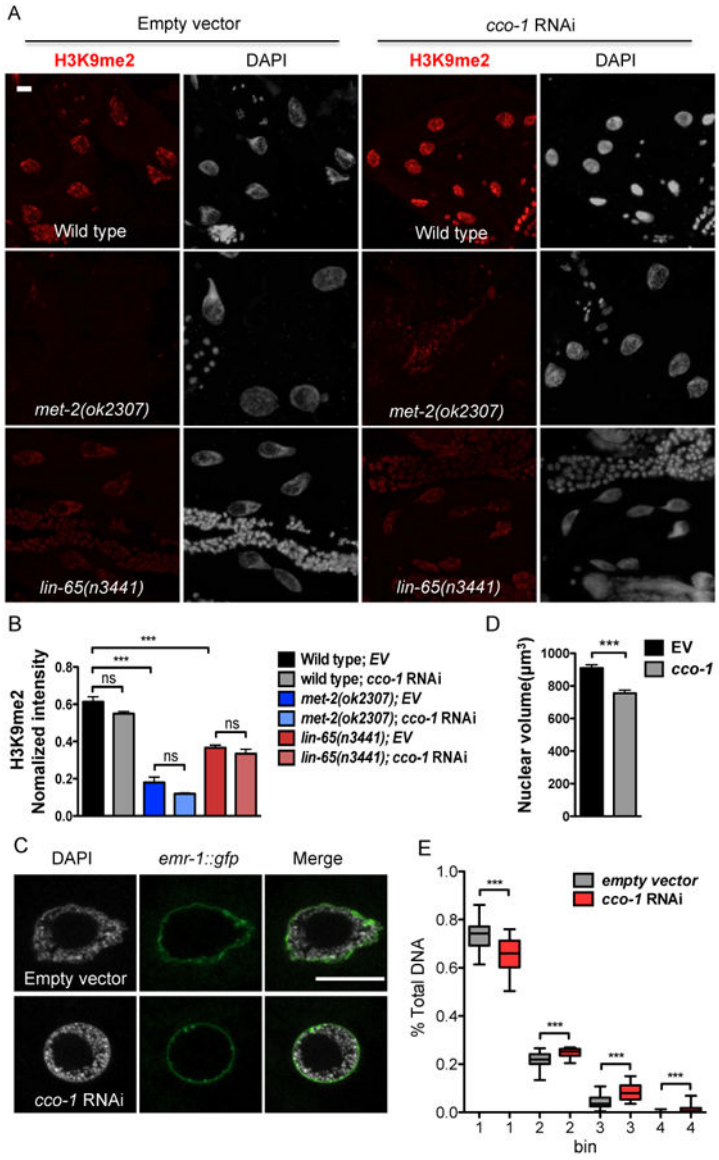

Figure 3. Mitochondrial stress induced chromatin reorganization

(A) Representative maximal intensity projection images of H3K9me2 immunostaining of intestinal nuclei in Day 1 adult WT, *met-2* or *lin-65* mutant animals grown on EV or *cco-1* RNAi from hatch (as indicated). H3K9me2 (Red); DAPI (Grey). Scale bar represents 10 μm.

(B) Quantification of H3K9me2 level. The genotypes and treatments are as in (A). H3K9me2 intensity is normalized to DAPI intensity. (*** denotes $p < 0.0001$; ns denotes $p > 0.05$ via t-test, error bars indicate SEM, $n \geq 15$ nuclei)

(C) Representative of 3 center images of DAPI staining with *lmn-1p::emr-1::gfp* of intestinal nuclei in Day 1 adult animals grown on EV or *cco-1* RNAi from hatch as indicated. *lmn-1p::emr-1::gfp* (Green); DAPI (Grey). Scale bar represents 10 μm.

(D) Quantification of the intestinal nuclear size at Day 1 adulthood using *lmn-1p::emr-1::gfp* as a marker. Animals grown on EV or *cco-1* RNAi from hatch (*** denotes $p < 0.0001$ via t-test, error bars indicate SEM, $n \geq 20$ nuclei)

(E) Quantification of the distribution of DAPI staining signal in intestinal nuclei at Day 1 of adulthood in animals grown on EV or *cco-1* RNAi from hatch. The distribution of fractions from the top four bins are shown as boxplots. (*** denotes $p < 0.0001$ via mann-whitney test, error barsindicate SEM, $n \geq 25$ nuclei)

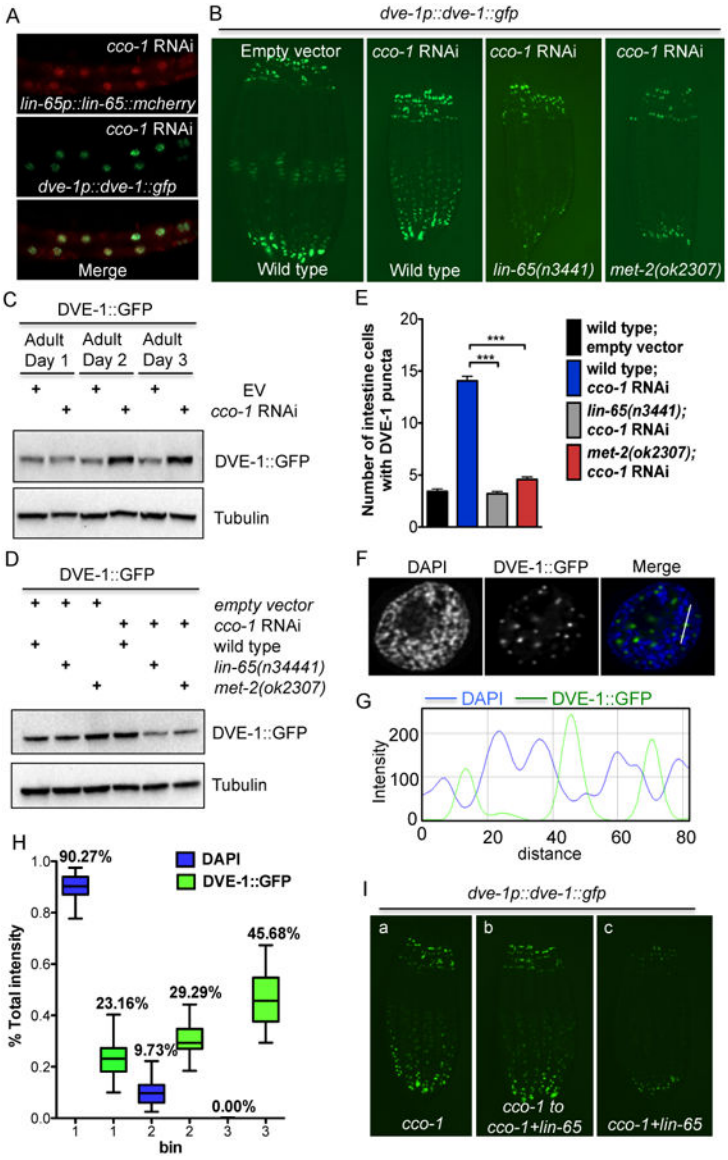

Figure 4. DVE-1 nuclear distribution upon mitochondrial stress is dependent on *lin-65* and *met-2*

(A) Representative photomicrographs of Day 1 adult animals expressing both *lin-65p::lin-65::mCherry* and *dve-1p::dve-1::gfp* grown on *cco-1* RNAi from hatch.

(B) Representative photomicrographs of Day 1 *dve-1p::dve-1::gfp* animals in *wild type*, *lin-65* and *met-2* background grown on EV or *cco-1* RNAi from hatch.

(C) Immunoblot of GFP expression in WT animals grown on EV or *cco-1* RNAi from hatch. Animals were collected at Day 1, 2 and 3 of adulthood. Anti-tubulin serves as a loading control.

(D) Immunoblot of GFP expression in Day 1 adult animals in WT, *lin-65* or *met-2* mutant background grown on EV or *cco-1* RNAi from hatch. Anti-tubulin serves as a loading control.

(E) Quantification of the number of intestinal nuclei with DVE-1 puncta structure per worm. The genotypes and treatments are as in (B). (*** denotes $p < 0.0001$ via t-test, error bars indicate SEM, $n \geq 30$ worms). See also Figure S4D.

(F) Representative photomicrographs of DVE-1: :GFP punctate structure in one intestinal nucleus. DVE-1: :GFP (Green); DAPI (Blue).

(G) The intensity profile of both DAPI and DVE-1: :GFP across the white line as shown in Figure 4F.

(H) Quantification of the distribution of DVE-1: :GFP signal in nuclei with DAPI staining. DVE-1: :GFP animals grown on *cco-1* RNAi from hatch. The distribution of fractions of all three bins are shown as boxplots ($n \geq 30$ nuclei).

(I) Representative photomicrographs of DVE-1: :GFP expression in animals grown on : (a) *cco-1* RNAi for 5 days from hatch; (b) *cco-1* RNAi for 3 days from hatch and then transferred to *cco-1+lin-65* double RNAi for 2 more days; (c) *cco-1+lin-65* double RNAi from L4, F1 generations were examined.

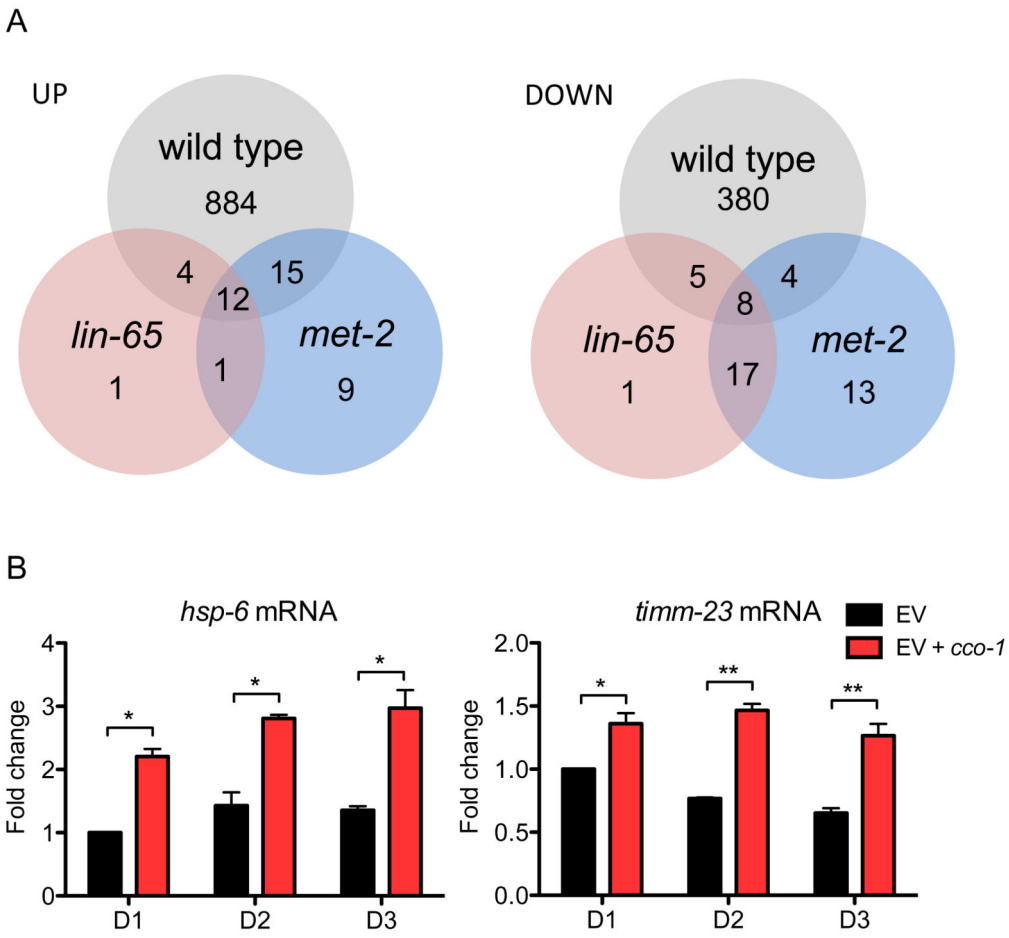

Figure 5. Gene expression changes upon *cco-1* RNAi treatment is strongly dependent upon *lin-65* and *met-2*

(A) Venn diagram of numbers of differentially expressed genes in wild type, *lin-65* and *met-2* mutant animals grown on *cco-1* RNAi for 2 days. Genes with an adjusted P-value < 0.05 were selected as differentially expressed genes. See also Table S2.

(B) Quantitative PCR of *hsp-6* and *timm-23* mRNA level. Synchronized Day1, 2 and 3 adult animals grown on EV or EV+*cco-1* RNAi from hatch were collected for qPCR. (* denotes $p < 0.05$, ** denotes $p < 0.01$ via t-test, error bar indicates the SEM from three biological replicates)

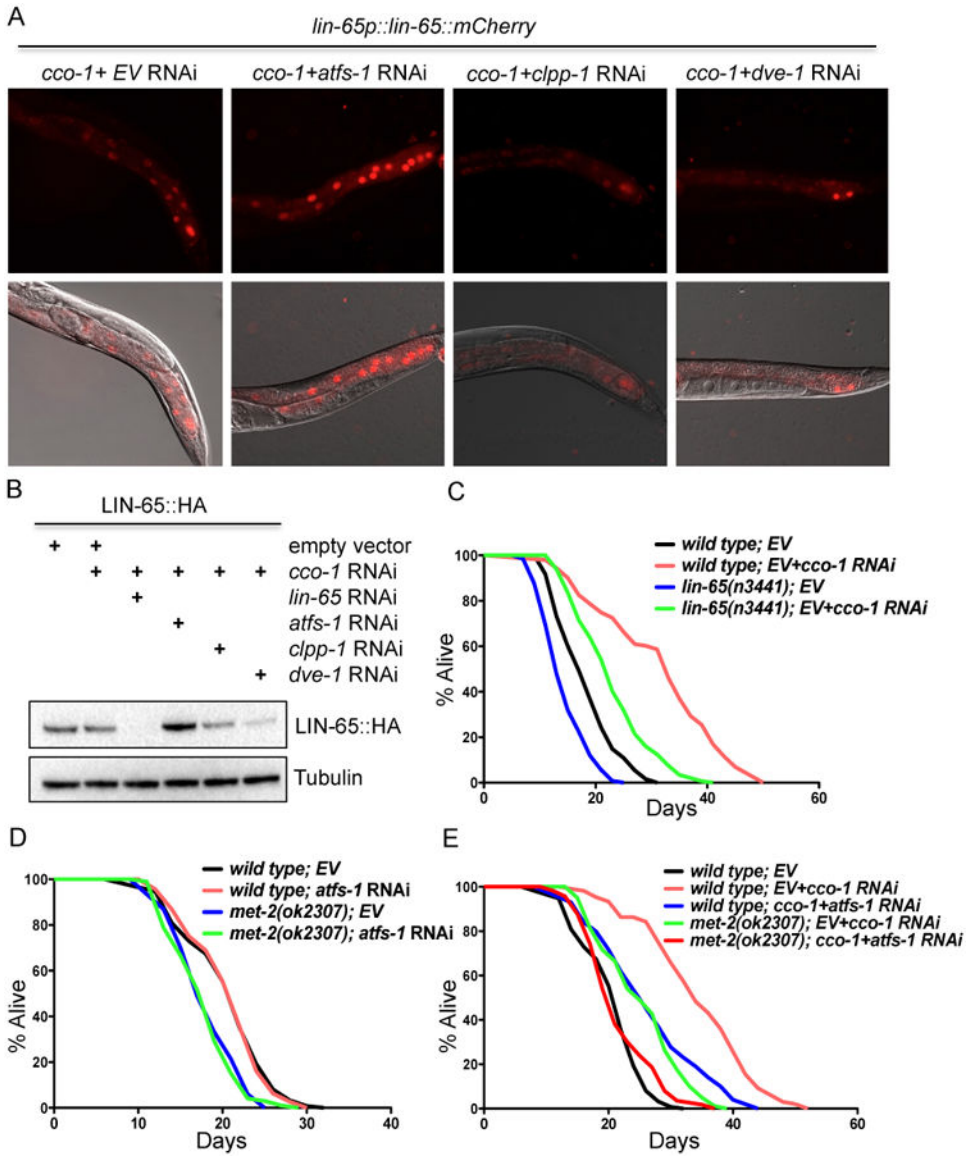

Figure 6. Mitochondrial stress-induced LIN-65 nuclear translocation is partially dependent on *clpp-1* and *dve-1*, but independent of *atfs-1*

(A) Representative photomicrographs of Day 1 adult animals expressing *lin-65p::lin-65::mCherry* grown on RNAi from hatch as indicated.

(B) Immunoblot of against HA-tag in LIN-65::HA animals grown on RNAi bacteria from hatch (as described in (A)). Animals were collected at Day 1 of adulthood. Anti-tubulin serves as a loading control.

(C) Survival analyses of *lin-65(n3441)* animals on EV or EV+*cco-1* RNAi. See Table S1 for lifespan statistics.

(D) Survival analyses of *met-2(ok2307)* animals on EV or *atfs-1* RNAi. See Table S1 for lifespan statistics.

(E) Survival analyses of *met-2(ok2307) and atfs-1* RNAi treated animals under mitochondrial stress condition with *cco-1* RNAi. See Table S1 for lifespan statistics.

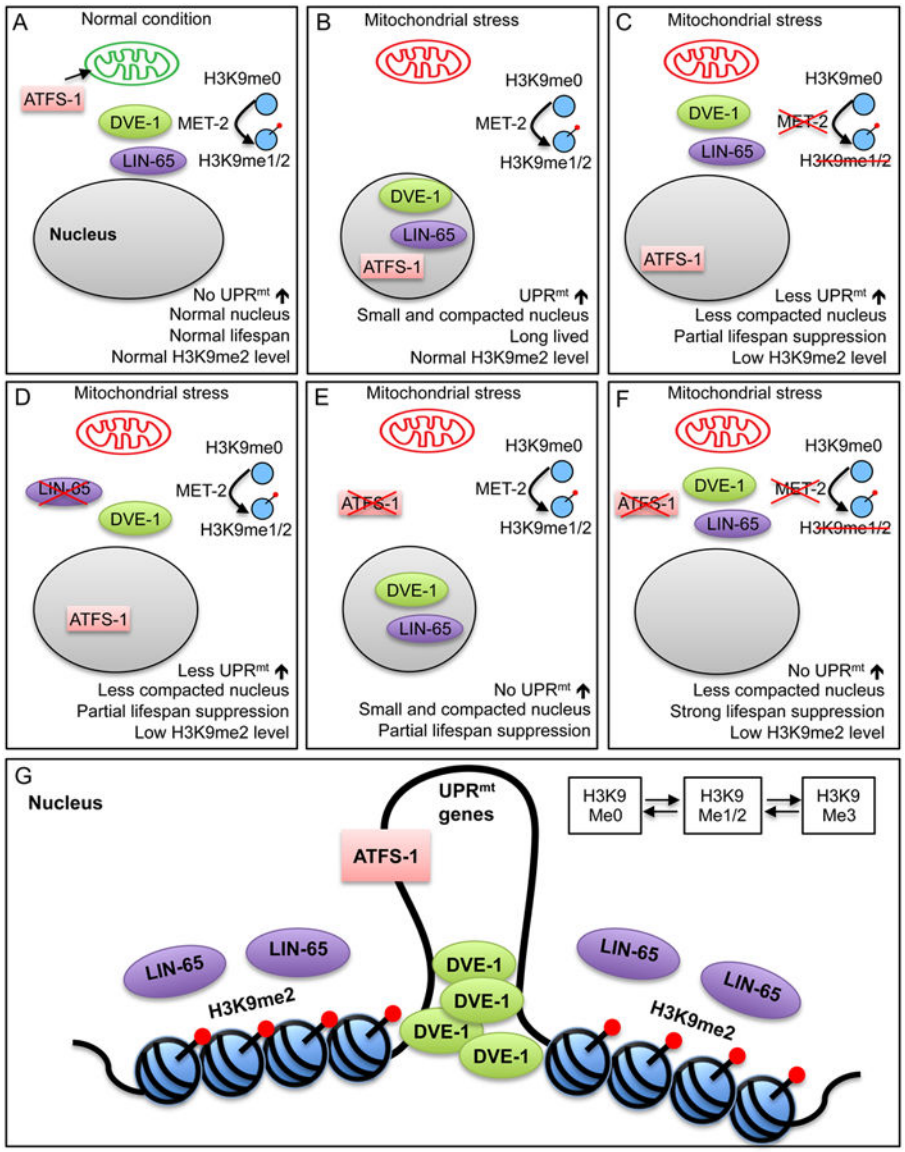

Figure 7. Model for mitochondrial stress signaling pathway

(A) Under non-stressed conditions, MET-2 produces H3K9me1/2 histone subunits in the cytoplasm. ATFS-1 translocates to the mitochondria and is degraded. DVE-1 and LIN-65 do not accumulate in the nucleus and the UPR^{mt} is not induced, animals are normal lived and the nucleus is not compacted (Figure 3A).

(B) During mitochondrial stress, MET-2 continues to produce H3K9me2 histone subunits, ATFS-1 now translocates to the nucleus to induce UPR^{mt}. DVE-1 and LIN-65 accumulate in the nucleus (Figure 2A-C and Figure 4B-D). Animals are long-lived, the UPR^{mt} is induced, nuclei become compacted (Figure 3A), and H3K9me2 levels remain unchanged (Figure 3B).

(C) Loss of *met-2* during mitochondrial stress results in reduced nuclear H3K9me2 levels, nuclei that are less compacted (Figure 3A), reduced DVE-1 and LIN-65 nuclear accumulation (Figure 2A and Figure 4B), reduced UPR^{mt} induction (Figure S1B) and partial suppression of increased lifespan (Figure 6E).

(D) Loss of *lin-65* during mitochondrial stress results in reduced nuclear H3K9me2 levels (Figure 3B), nuclei that are less compacted (Figure 3A), reduced DVE-1 nuclear accumulation (Figure 4B), reduced UPR^{mt} induction (Figure 3A and Figure S1B) and partial suppression of increased lifespan (Figure 6C).

(E) Loss of *atfs-1* during mitochondrial stress results in suppressed UPR^{mt} induction (Figure 1A) and partial suppression of lifespan extension (Figure 6E). This is independent of compacted nuclei (Figure S7B) and nuclear accumulation of DVE-1 and LIN-65 (Figure 6A and 6B).

(F) Loss of both *met-2* and *atfs-1* during mitochondrial stress results in nuclei that are less compacted, reduced nuclear accumulation of DVE-1 and LIN-65, no UPR^{mt} induction and complete suppression of lifespan extension. (Figure 6E).

(G) During mitochondrial stress, LIN-65 and DVE-1 accumulate in the nucleus, chromatin becomes remodeled, and DVE-1 is able to form puncta at the loose regions of the chromatin, activating transcription of UPR^{mt} targets. This remodeling works in parallel to the relocation of mitochondrial specific transcription factor ATFS-1 to initiate UPR^{mt} and regulate longevity.